TRENDS IN SCIENCES 2026; 23(9): 12818
https://doi.org/10.48048/tis.2026.12818
RESEARCH ARTICLE

# Optimizing Transfersome Delivery of Single-Aged Garlic Extract: A Comparative Study of Characterization, Phytochemical Content, and Antibacterial Potency

**Sri Rahayu Lestari[1,*], Dewi Sekar Miasih[2], Alif Rosyidah El Baroroh[1], Yuslinda Annisa[3,4], Muhammad Mauludi Zulkifli[1], Abdul Gofur[1], Yunita Rakhmawati[1], Suharti[5] and Nik Ahmad Nizam Nik Malek[6,7]**

*[1]Department of Biology, Faculty of Mathematics and Natural Science, Universitas Negeri Malang, Malang 65145, Indonesia*
*[2]Cardiovascular Research Center, Faculty of Medicine, Universitas Brawijaya, Malang 65145, Indonesia*
*[3]Department of Biology, Faculty of Mathematics and Natural Sciences, Universitas Brawijaya, Malang 65145, Indonesia*
*[4]Innovation Center of Integrative Jamu and Eco-pharmaca, Universitas Brawijaya, Malang 65145, Indonesia*
*[5]Department of Chemistry, Faculty of Mathematics and Natural Science, Universitas Negeri Malang, Malang 65145, Indonesia*
*[6]Department of Biosciences, Faculty of Biosciences, Universiti Teknologi Malaysia, Johor Bahru 81310, Malaysia*
*[7]Centre for Sustainable Nanomaterials (CSNano), Ibnu Sina Institute for Scientific and Industrial Research (ISI-ISIR), Universiti Teknologi Malaysia, Johor Bahru 81310, Malaysia*

**([*]Corresponding author's e-mail: srirahayulestari@um.ac.id)**

*Received: 26 November 2025, Revised: 14 January 2026, Accepted: 24 January 2026, Published: 30 March 2026*

**Abstract**

Skin infections remain a significant global health concern, particularly with the increasing prevalence of antibiotic-resistant pathogens. Single-aged garlic (SAG), a fermented form of *Allium sativum*, possesses enhanced antioxidant and antibacterial properties due to its enriched phenolic and flavonoid content. This study aimed to optimize and characterize the transfersome-based delivery system of SAG extract (T-SAG), and to evaluate its physicochemical properties, phytochemical content, antioxidant activity, and antibacterial potency. SAG was produced through controlled thermal incubation followed by microwave-assisted extraction, and subsequently formulated into transfersomes using the thin-film hydration method with phosphatidylcholine and sodium deoxycholate as an edge activator. The formulation was characterized in terms of particle size, polydispersity index (PDI), zeta potential, encapsulation efficiency, morphology, chemical compatibility, and storage stability. The optimized transfersome formulation exhibited nanosized vesicles (81.03 ± 0.47 nm) with a low PDI (0.14 ± 0.008), a zeta potential of −17.93 ± 0.31 mV, and high encapsulation efficiency (77.04 ± 6.62%). Transmission electron microscopy revealed well-defined spherical vesicles with uniform size distribution, while scanning electron microscopy confirmed smooth surface morphology and structural integrity. Fourier-transform infrared spectroscopy indicated no significant chemical interactions between SAG and lipid components, confirming successful encapsulation. Stability studies conducted over 28 days at 4 °C demonstrated minimal changes in particle size and zeta potential. Phytochemical analysis showed total phenolic and flavonoid contents of 62.19 ± 1.07 mg GAE/g and 63.15 ± 0.38 mg QE/g, respectively, accompanied by strong antioxidant activity (77.74 ± 2.88% DPPH inhibition). Antibacterial activity, evaluated using the Kirby-Bauer disk diffusion method against *Escherichia coli*, *Staphylococcus aureus*, and *Pseudomonas aeruginosa*, demonstrated notable inhibitory effects, particularly against *E. coli* (8.19 ± 1.34 mm), with chloramphenicol used as a positive control. These findings indicate that transfersome-based delivery enhances the stability and bioactivity of SAG extract, supporting its potential application as a natural topical antimicrobial formulation.

**Keywords:** Antibacterial potency, Characterization, Phytochemical content, Single-aged garlic, Transfersome

**Introduction**

Skin infections and chronic wounds caused by pathogenic bacteria such as *Staphylococcus aureus*, *Escherichia coli*, and *Propionibacterium acnes* remain a significant global health concern [1]. According to the World Health Organization (WHO), approximately 15% of hospitalized patients experience nosocomial infections, with skin infections accounting for a substantial proportion, especially in developing countries [2,3]. In Indonesia, evidence from the 2018 National Basic Health Research (Riskesdas) and institutional reports from Dr. Soetomo General Hospital (Surabaya, East Java) suggests that skin and soft tissue infections are a major cause of hospitalization in patients with diabetic wounds [4]. Diabetic foot ulcers affect approximately 15% - 25% of diabetic patients, with amputation rates reaching 20% - 25% due to uncontrolled infections [5,6]. Over the past decade, increasing antibiotic resistance among skin pathogens, particularly against topical agents such as gentamicin, mupirocin, and chloramphenicol, has markedly reduced treatment effectiveness and heightened the risk of recurrent infection and progression to systemic complications [7]. Hypersensitivity reactions to conventional antibiotics have also been frequently reported, highlighting the urgent need for safer and more sustainable therapeutic alternatives [8]. In this context, natural antibacterial agents such as plant extracts are gaining attention as promising strategies for topical antimicrobial therapies.

Single-Aged Garlic (SAG), the fermented form of *Allium sativum*, has been extensively studied over the past ten years for its enhanced antibacterial and antioxidant properties compared to fresh garlic [9-11]. The fermentation process boosts beneficial compounds like S-allyl cysteine (SAC) and flavonoids, which are effective at fighting off common skin germs [12]. Several studies have reported that Single-Aged Garlic (SAG) extract inhibits the growth of *E. coli* and *S. aureus*, producing inhibition zones of up to 24 mm, and also suppresses *P. acnes*, a bacterium implicated in acne pathogenesis [13,14]. Furthermore, SAG has shown antimicrobial potential in personal hygiene products, with inhibition zones of 12.7 mm against *E. coli*, indicating its broad applicability [13]. Despite its promise, challenges remain regarding the stability of active compounds, skin penetration, and effectiveness in topical applications. These limitations require the use of advanced delivery systems to improve how well SAG-derived ingredients work in the body and their efficacy in treating conditions.

One of the most promising topical delivery systems is the transfersome, a highly deformable lipid-based vesicle that can efficiently penetrate the stratum corneum [15]. Transfersomes improve dermal absorption due to their high deformability, which is achieved by incorporating edge activators such as surfactants [16]. Recent studies have shown that sodium deoxycholate, as an edge activator, can produce more deformable and stable vesicles, enabling higher skin penetration compared to conventional surfactants like Tween 80 or Span 60 [17,18]. However, the use of sodium deoxycholate-based transfersomes for natural actives such as SAG remains limited, particularly in the context of treating resistant skin infections. Therefore, innovation in transfersome formulation components is crucial for developing effective herbal-based topical treatments.

In this study, the thin-film hydration method was chosen because it creates even and stable vesicles, especially when using absolute ethanol as a solvent [19,20]. Absolute ethanol helps create a better lipid film and improves how well the vesicles hold their contents and stay stable [21,22]. Despite its advantages, the application of absolute ethanol to herbal-based transfersome preparations is still underexplored. The integration of SAG extract, rich in antibacterial compounds; sodium deoxycholate as a deformability enhancer; and absolute ethanol as a solvent offers a novel and strategic approach to developing superior topical drug delivery systems. Beyond physical formulation, evaluating the phytochemical content of active compounds is essential in herbal-based topical product development. This study assesses total phenolic content (TPC) and total flavonoid content (TFC) in the SAG extract-loaded transfersomes. Phenolic and flavonoid compounds are known to help fight bacteria by blocking enzymes, breaking down bacterial cell membranes, and causing oxidative stress [11,23,24]. Quantitative analysis of these compounds allows for the correlation between phytochemical characterization and the biological activity of the formulation, revealing

detailed information about both physical and pharmacological performance.

In addition to characterizing the phytochemical content and physical properties of the formulation, this study also evaluates its antibacterial performance against key skin pathogens, namely *S. aureus*, *E. coli*, and *P. acnes*. Antibacterial assays were conducted to compare the inhibitory activity of SAG-transfersomes with non-vesicular SAG extracts and standard controls. This integrative approach not only highlights the importance of nanocarrier-based systems in enhancing bioactivity, but also provides evidence for the added value of combining strategic formulation components. Given the increasing challenge of antibiotic resistance and the need for effective topical herbal therapies, such comparative evaluation is essential. Therefore, this study aims to optimize transfersome-based delivery of single-aged garlic (SAG) extract and to evaluate its physicochemical properties, phytochemical content including total phenolic content (TPC) and total flavonoid content (TFC), and antibacterial activity. The results are expected to provide a robust basis for developing safe, stable, and effective topical antimicrobial formulations derived from plant-based bioactives.

## Materials and methods

### Materials

Single clove garlic (*Allium sativum* L.) was collected from Sarangan Village, Magetan District, East Java, Indonesia. Absolute ethanol, phospholipid (phosphatidylcholine), sodium deoxycholate, and DPPH were obtained from Sigma-Aldrich (Germany). Sodium nitrate ($NaNO_3$), sodium hydroxide (NaOH), sodium carbonate ($Na_2CO_3$), and Folin–Ciocalteu reagent were purchased from Merck (Germany). Aluminum chloride ($AlCl_3$) was obtained from Smart Lab (Indonesia). Quercetin and gallic acid were used as reference standards. All chemicals were of analytical grade and used without further purification.

### Instrumentation

Particle size distribution, polydispersity index (PDI), and zeta potential were analyzed using a Particle Size Analyzer (Horiba SZ-100Z, Japan). Morphological characterization was performed using transmission electron microscopy (TEM; JEOL JEM-1400, Japan) and scanning electron microscopy (SEM; Hitachi, Japan). UV-Vis spectrophotometric measurements were conducted using a Biochrom Libra S11/12 spectrophotometer (UK). A magnetic stirrer, ultrasonic cleaner, rotary evaporator, freeze dryer, and temperature-controlled water bath were employed during formulation and analysis procedures.

### Preparation of Single-Aged Garlic (SAG) extract

Fresh single garlic was cleaned from residual impurities and incubated at 75 °C for 21 days. During the incubation process, the garlic gradually darkened in color, resulting in a blackish-brown appearance, indicating the formation of Single-Aged Garlic (SAG). The aged garlic was peeled, crushed, and subjected to microwave-assisted extraction (MAE). The crushed SAG was mixed with absolute ethanol at a ratio of 1:10 (w/v) and extracted using a microwave reaction system (Multiwave PRO, Anton Paar, Austria) at 50 °C for 10 min with a power of 1,500 W. The extract was filtered, concentrated under reduced pressure using a rotary evaporator at 37 °C, and further dried in an oven at 40 °C to obtain a solvent-free SAG extract.

### Preparation of SAG-Loaded Transfersomes (T-SAG)

Transfersomes were prepared using a modified thin-film hydration method as described by Jiang *et al.* [25]. Phosphatidylcholine (0.167 g) and sodium deoxycholate (0.033 g) were dissolved in absolute ethanol and stirred at 50 °C for 1 h. The solvent was evaporated to form a thin lipid film, which was subsequently hydrated with phosphate-buffered saline (PBS) containing 0.01 g of SAG extract. The resulting suspension was sonicated for 30 min, magnetically stirred for an additional hour, and stored at 4 °C until further characterization.

### Characterization of T-SAG

Transfersome samples were analyzed without prior dilution. Prior to analysis, the samples were sonicated in a bath sonicator for 5 min to minimize aggregation and ensure uniform dispersion, as commonly performed in nanocarrier characterization [26]. The measurement was conducted at the Water Technology and Industrial Consulting Laboratory,

Department of Chemical Engineering, Institut Teknologi Sepuluh Nopember (ITS), Surabaya. A Particle Size Analyzer (Horiba SZ-100Z, Japan) was used to determine the average particle diameter (Z-average), polydispersity index (PDI), and zeta potential. Each measurement was performed in triplicate under ambient conditions.

**Transmission Electron Microscopy (TEM)**

Morphological analysis of the transfersome containing T-SAG was conducted using TEM (JEOL JEM-1400, Japan). A drop of undiluted T-SAG sample was placed on a carbon-coated copper grid and allowed to adsorb for 1 - 2 min. Excess fluid was gently removed with filter paper, and the sample was negatively stained with 2% (w/v) phosphotungstic acid (PTA) for 30 s. The grid was then air-dried at room temperature before examination. This sample preparation method was adapted from recent protocols commonly applied in nanovesicle morphology studies [27,28]. TEM analysis was carried out at the Chemistry Laboratory, Faculty of Mathematics and Natural Sciences, Universitas Gadjah Mada, Yogyakarta, Indonesia.

**Scanning Electron Microscopy (SEM)**

T-SAG samples were freeze-dried using a freeze dryer (Christ Alpha 1 - 2 LDplus, Germany) at –20 °C for 24 h to obtain the powdered form. Prior to analysis, approximately 0.5 g of the freeze-dried powder was mounted on a brass pedestal and coated with a thin layer of gold using a sputter coater. Surface morphology was then examined using a SEM (Hitachi, Tokyo, Japan) at the Laboratory of Mechanical Engineering, Faculty of Industrial Technology, Institut Teknologi Sepuluh Nopember (ITS), Surabaya. The SEM images were used to evaluate the surface texture and structural characteristics of the T-SAG particles [29].

**Fourier Transform Infrared Spectroscopy (FTIR)**

FTIR analysis was performed to identify the functional groups in the samples. About 2 mg of the sample was analyzed using an infrared spectrophotometer (Shimadzu IR Spirit-T, equipped with Shimadzu LabSolutions IR software, Japan). The measurement was carried out with 10 scans at a resolution of 4 $cm^{-1}$. Data were collected in the range of 4,000 - 400 $cm^{-1}$ under ambient conditions [30,31].

**Encapsulation Efficiency (EE)**

EE was determined as the percentage of TPC successfully encapsulated within the transfersomes, as described by Tagrida *et al.* [32]. The separation of unencapsulated extract from the transfersomal suspension was performed by centrifugation at 12,000×g for 30 min at 4 °C using a refrigerated centrifuge (Diagen-21, Orto Alresa, Spain). The resulting pellet was rinsed with deionized water and recentrifuged under the same conditions. The purified transfersome pellet was then resuspended in deionized water and adjusted to a final volume of 2 mL. To release the encapsulated phenolic compounds, the vesicle membranes were disrupted by mixing 1 mL of the transfersome suspension with 1 mL of 0.02% (v/v) Triton X-100 solution, followed by incubation. Similarly, 1 mL of the collected supernatant (representing the unencapsulated phenolics) was mixed with 1 mL of 2% Triton X-100 solution to standardize the measurement conditions. The concentration of phenolic compounds in both the disrupted transfersome (P) and the supernatant (S) was quantified using the Folin-Ciocalteu method, measured spectrophotometrically at 765 nm. The encapsulation efficiency was then calculated using the following formula:

$$\%EE = \frac{P}{S+P}\ x\ 100\% \quad (1)$$

where P is the amount of phenolic compounds released from the transfersomes after disruption with Triton X-100, and S is the amount of free phenolic compounds present in the supernatant. Each measurement was performed in triplicate.

**Stability study**

A total of 10 mL of freshly prepared T-SAG-loaded transfersome suspension was transferred into sterile 15 mL conical tubes and sealed tightly. The samples were stored under 2 different conditions, 4 °C (refrigerated) and 25 °C (room temperature), for 4 weeks. Stability was evaluated by measuring the particle size, PDI, and zeta potential at week 0 and week 4. All parameters were assessed using a particle size analyzer under ambient laboratory conditions. This procedure was performed with reference to the method described

by Hadidi *et al.* [33], with slight modifications. Each measurement was performed in triplicate.

**2,2-diphenyl-1-picrylhydrazyl (DPPH) antioxidant activity**

The antioxidant activity of the samples was evaluated using the DPPH radical scavenging assay, with slight modifications [30]. A 50 µM DPPH solution was prepared by dissolving DPPH powder (Sigma-Aldrich, Germany) in methanol. Transfersome samples were mixed with the DPPH solution in a 1:5 ratio (v/v), followed by incubation in the dark at room temperature for 15 min. The absorbance of the reaction mixture was then measured at 517 nm using a UV-Vis spectrophotometer (Biochrom 12S, UK). The percentage of radical scavenging activity (% inhibition) was calculated using the following equation:

$$\% \text{ inhibition} = \frac{A0 - A1}{A0} \times 100 \quad (2)$$

where A0 represents the absorbance of the DPPH solution without sample (control), and A1 represents the absorbance of the sample-DPPH mixture after incubation. Each measurement was performed in triplicate.

**Total Flavonoid Content (TFC)**

To determine the total flavonoid content, 200 µL of transfersome sample was mixed with 280 µL of distilled water and 60 µL of 5% $NaNO_3$ (Merck, Germany), then incubated for 5 min at room temperature in the dark. After incubation, 60 µL of 10% $AlCl_3$ (Smart Lab, Indonesia) was added and the mixture was left to react for 6 min under light-protected conditions. The reaction was terminated by adding 400 µL of 1 M NaOH (Merck, Germany), and the final volume was gently homogenized. Samples containing flavonoids formed a yellow-colored complex. The absorbance was measured at 510 nm using a UV-Vis spectrophotometer, and flavonoid concentration was determined based on a standard calibration curve constructed from quercetin solutions (Sigma-Aldrich, Germany) in the concentration range of 1 - 50 mg/L [34]. Each measurement was performed in triplicate. Total flavonoid content was expressed as quercetin equivalent (QE), representing the amount of quercetin in micrograms equivalent to 1 gram of sample (µg QE/g).

**Total Phenol Content (TPC)**

The TPC of the samples was determined using the Folin-Ciocalteu method. A volume of 400 µL of the sample was mixed with 400 µL of 10% Folin-Ciocalteu reagent (Merck, Germany) and incubated for 5 min at room temperature. Subsequently, 300 µL of 75 g/L $Na_2CO_3$ solution (Merck, Germany) was added, and the mixture was further incubated in the dark for 60 min. The absorbance was measured at 760 nm using a UV-Vis spectrophotometer. Each measurement was performed in triplicate. TPC values were quantified using a standard calibration curve constructed from gallic acid (Sigma-Aldrich, Germany) solutions at concentrations ranging from 1 to 50 mg/L, and results were expressed as gallic acid equivalent (GAE), indicating the microgram amount of gallic acid equivalent per gram of sample (µg GAE/g).

**Antibacterial activity assay**

The antibacterial activity of the samples was evaluated using the Kirby-Bauer disk diffusion method on Mueller–Hinton Agar (MHA) (Oxoid, UK), following Clinical and Laboratory Standards Institute (CLSI) guidelines. The bacterial strains used in this study were *Pseudomonas aeruginosa* (ATCC 27853), *Staphylococcus aureus* (ATCC 25923), and *Escherichia coli* (ATCC 25922), obtained from the Surabaya Center for Health Laboratory (BBLK, Surabaya, Indonesia) and maintained on nutrient agar slants. Each bacterial isolate was inoculated into nutrient broth and incubated at 37 °C for 24 h. The turbidity of the bacterial suspensions was adjusted to the 0.5 McFarland standard (approximately $1.5\times10^8$ CFU/mL). The standardized suspensions were evenly spread onto the surface of MHA plates using sterile cotton swabs.

Transfersome-loaded SAG (T-SAG) was tested at concentrations of 100, 150 and 200 mg/mL. Chloramphenicol (1 mg/mL) was included solely as a positive control to confirm bacterial susceptibility and to validate the performance of the disk diffusion assay, in accordance with CLSI recommendations. The antibacterial activity of T-SAG was not intended to be directly compared with chloramphenicol. Sterile paper disks (6 mm diameter) were immersed in each test solution for 15 min and then placed onto the inoculated

agar surfaces. The plates were incubated at 37 °C for 24 h. After incubation, the diameters of the inhibition zones were measured in millimeters using a digital caliper [35]. Each measurement was performed in triplicate. All tests were performed under identical experimental conditions.

## Results and discussion

### Characterization and Stability of T-SAG Formulation

Characterization of T-SAG was evaluated based on particle size (Z-average), PDI, and zeta potential before and after 4 weeks of storage at 4 and 25 °C, as summarized in **Table 1** and **Figure 1**. The initial PDI value of T-SAG stored at 25 °C was 0.140 ± 0.008, indicating a narrow and homogeneous particle size distribution, which is favorable for colloidal stability [30]. However, after 4 weeks, the PDI increased to 0.324 ± 0.034, while storage at 4 °C resulted in an even higher PDI of 0.694 ± 0.035, suggesting greater heterogeneity and potential vesicle aggregation [36]. PDI values above 0.4 typically denote broad size distributions, which can negatively affect formulation stability [37]. This increase may result from vesicle fusion or restructuring, possibly influenced by the ratio of phosphatidylcholine and sodium deoxycholate as membrane-forming and edge-activating agents [16,17]. Sodium deoxycholate, while enhancing vesicle flexibility and skin penetration, can disrupt lipid bilayer uniformity, especially during storage [17].

**Table 1** Characterization of T-SAG based on PDI, Z-average, and zeta potential before and after storage.

| Time | Temperature 4 °C | | | Temperature 25 °C (Room Temperature) | | |
|---|---|---|---|---|---|---|
| | PDI | Z-average (nm) | Zeta Potential (mV) | PDI | Z-average (nm) | Zeta Potential (mV) |
| 0 W | NA | NA | NA | 0.140 ± 0.008 | 81.033 ± 0.473 | −17.933 ± 0.306 |
| 4 W | 0.694 ± 0.035 | 277.900 ± 9.429 | −16.240 ± 0.997 | 0.324 ± 0.034 | 512.600 ± 1.629 | −13.540 ± 0.218 |

Note: NA (not analyzed); W (week of storage); T-SAG (Transfersomes Single-Aged Garlic); PDI (Polydispersity Index).

These changes collectively demonstrate that T-SAG vesicles are prone to physicochemical instability over time, particularly under ambient storage. The increase in both PDI and particle diameter indicates that vesicle fusion, swelling, or structural rearrangement may have occurred, likely due to lipid bilayer destabilization [38]. Phosphatidylcholine, the primary structural lipid, typically forms stable bilayers. However, in the presence of ethanol, which acts as both a penetration enhancer and a membrane fluidizer, bilayer rigidity may decrease, thereby facilitating vesicle deformation and, in some cases, coalescence [39]. Moreover, sodium deoxycholate, acting as an edge activator, disrupts lipid packing at the bilayer margins [1]. While this facilitates transdermal delivery by increasing membrane fluidity, it also compromises vesicle integrity during prolonged storage, particularly at elevated temperatures.

The Z-average values in **Table 1** show that freshly prepared T-SAG at 25 °C had a mean particle size of 81.033 ± 0.473 nm, which is within the optimal nanoscale range (10 - 200 nm) for transdermal drug delivery systems [40,41]. After 4 weeks of storage, the vesicle size increased substantially to 512.600 ± 1.629 nm at 25 °C and 277.900 ± 9.429 nm at 4 °C, indicating vesicle enlargement and potential aggregation [42]. This enlargement may result from decreased membrane rigidity due to ethanol loss or lipid degradation over time [26,38]. An increase in particle size not only compromises the physical stability of the formulation but may also hinder its ability to penetrate the stratum corneum effectively, thus reducing delivery efficiency.

In terms of zeta potential, the surface charge of T-SAG decreased over time. At 0 week, the zeta potential of T-SAG stored at 25 °C was –17.933 ± 0.306 mV, which declined to –13.540 ± 0.218 mV after 4 weeks. Storage at 4 °C yielded a final zeta potential of –16.240 ± 0.997 mV. Zeta potential values between ±10 and ±20 mV reflect limited electrostatic stabilization, making the vesicles more susceptible to aggregation due to inadequate repulsive forces [16,43]. The relatively low zeta potential may be attributed to the zwitterionic

nature of phosphatidylcholine and the mild anionic charge from sodium deoxycholate, which are insufficient to provide strong surface charge stabilization. Additionally, ethanol evaporation could influence the interfacial properties of vesicles, further reducing the electrostatic barrier and accelerating aggregation [16,17].

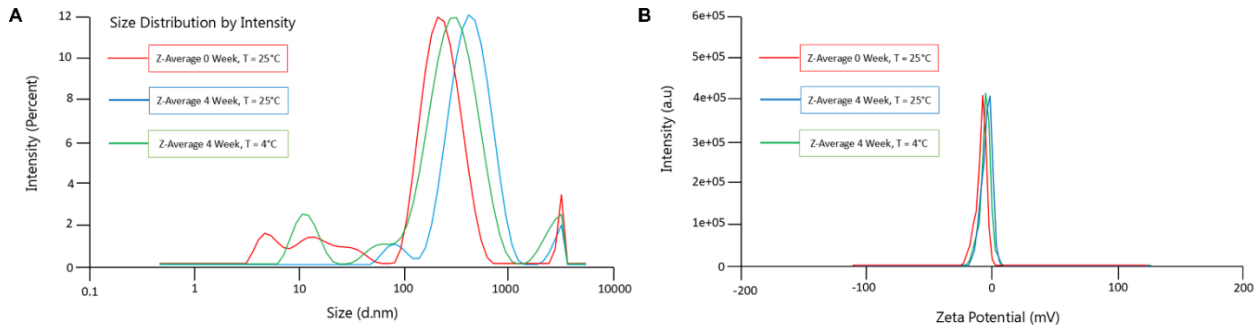


**Figure 1** Physicochemical characterization of T-SAG. (A) Z-average (hydrodynamic diameter); (B) zeta potential. T-SAG (Transfersomes Single-Aged Garlic).

Taken together, these findings highlight the pivotal influence of formulation composition and storage conditions on the physicochemical stability of T-SAG vesicles. The concurrent increase in particle size, broadening of size distribution, and reduction in zeta potential during storage, particularly at 25 °C, suggest that without formulation optimization and/or appropriate stabilizers, T-SAG may lose its nanoscale characteristics and colloidal stability. Accordingly, ensuring effective transdermal delivery requires careful optimization of phospholipid, surfactant, and penetration enhancer ratios, coupled with storage under suitable conditions.

**Transmission Electron Microscopy (TEM)**

TEM analysis revealed that the T-SAG formulation exhibited vesicular morphology with clearly defined spherical structures (**Figure 2**). **Figures 2(A)** and **2(B)** display individual vesicles observed at 20,000× and 40,000× magnifications, respectively. The observed particle in both images shows a well-formed, closed lipid bilayer, indicative of a unilamellar or oligolamellar vesicle [17]. The spherical appearance aligns with thermodynamically favored morphologies of phospholipid-based carriers, where lipid hydration leads to the spontaneous self-assembly into bilayer vesicles to minimize system free energy by reducing hydrophobic exposure to the aqueous environment [44]. This vesicle formation is driven by the amphiphilic nature of phosphatidylcholine, which orients its hydrophilic heads outward and hydrophobic tails inward, forming a bilayer that encloses an aqueous core [16].

Although **Figures 2(A)** and **2(B)** only depict single vesicles, they illustrate representative morphology. However, it is important to note that a uniform distribution cannot be fully confirmed based solely on individual particle images. Such morphological uniformity should be supported by complementary analytical data such as dynamic light scattering (DLS) results [45]. Although **Figures 2(A)** and **2(B)** only depict single vesicles, they illustrate representative morphology. However, it is important to note that a uniform distribution cannot be fully confirmed based solely on individual particle images. Such morphological uniformity should be supported by complementary analytical data such as DLS results [27], [46]. In this study, the freshly prepared T-SAG exhibited a PDI value of 0.140 ± 0.008, suggesting a narrow and homogeneous particle size distribution that favors colloidal stability [47]. After 4 weeks of storage at 25 °C, the PDI increased to 0.324 ± 0.034, which, although higher, still reflects an acceptable level of dispersion uniformity (below the 0.4 threshold) [43]. These changes were likely driven by lipid rearrangement or vesicle aggregation over time, as also indicated by the increase in Z-average. Therefore, the DLS results substantiate the morphological findings and confirm that, at the initial stage, the T-SAG vesicles were both structurally intact and relatively monodisperse.

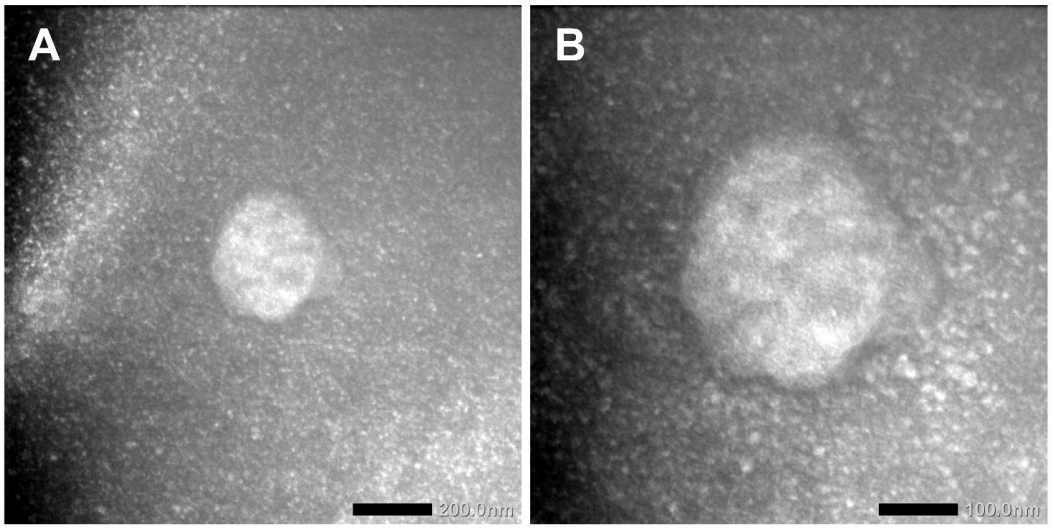


**Figure 2** Electron micrographs of T-SAG at (A) 20,000× and (B) 40,000× magnification. T-SAG (Transfersomes Single-Aged Garlic).

**Scanning Electron Microscopy (SEM)**

SEM was employed to investigate the surface morphology of freeze-dried T-SAG vesicles. SEM offers superior imaging capabilities over optical microscopy by providing enhanced depth of field and high-resolution visualization of particle surface characteristics, enabling detailed observation of topography, texture, and particle shape in the micrometer to nanometer range [48]. In contrast to TEM, which enables nanoscale visualization of internal ultrastructure in hydrated specimens, SEM is primarily used to evaluate surface morphology in the solid state, particularly following drying procedures such as lyophilization. [49]. In this study, the complementary use of both TEM and SEM provides a holistic understanding of T-SAG vesicle characteristics: TEM confirms the spherical and intact vesicle formation in suspension, while SEM evaluates the powder's physical structure, aggregation tendency, and redispersion potential during storage. As shown in **Figure 3** (SEM of T-SAG at 10,000× magnification), the surface morphology reveals a distribution of relatively uniform, spherical particles interspersed with occasional aggregates. These particles appear well-formed with smooth surfaces, supporting earlier characterization results such as PDI values below 0.4 in freshly prepared samples, indicating moderate monodispersity [50]. The observed aggregation may be attributed to the low zeta potential values, which suggest insufficient electrostatic repulsion to prevent vesicle clustering post-drying [16,37]. Additionally, the presence of some irregular or angular particles may result from lipid crystallization or vesicle fusion during the freeze-drying process [27].

The observed spherical morphology is typical of phospholipid-based systems like transfersomes [37]. Phosphatidylcholine, the main lipid component, self-assembles into bilayer vesicles upon hydration due to its amphiphilic nature, hydrophilic headgroups and hydrophobic tails, leading to energetically favorable spherical structures [51]. This morphology is crucial for transdermal drug delivery, as it enables vesicle deformability and skin penetration [16]. The flexibility of the vesicle membrane, supported by the presence of ethanol and sodium deoxycholate as membrane fluidizers and edge activators, allows the transfersomes to traverse the stratum corneum without compromising structural integrity [52]. Uniform and smooth vesicles enhance drug encapsulation efficiency, ensure consistent release profiles, and minimize batch-to-batch variation, key parameters in delivering bioactive compounds such as those found in SAG. Therefore, maintaining the spherical, non-aggregated morphology seen in SEM images is critical to ensuring the overall performance of T-SAG as a transdermal delivery system.

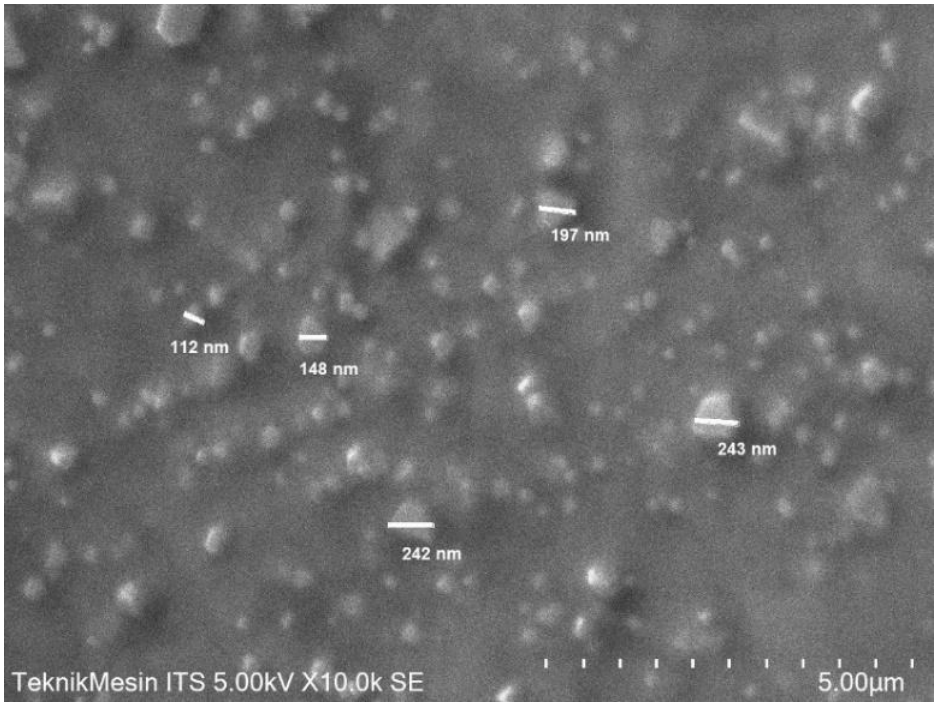


**Figure 3**. Scanning electron micrograph (SEM) of T-SAG at 10,000× magnification. Predominantly spherical particles (~100 - 250 nm) with minimal aggregation (SE detector, 5.00 kV). T-SAG (Transfersomes Single-Aged Garlic); SE (secondary electron).

**Fourier Transform Infrared Spectroscopy (FTIR)**

The FTIR spectrum of the SAG extract revealed the presence of characteristic functional groups associated with its phytochemical constituents. As illustrated in **Figure 4** and summarized in **Table 2**, a prominent absorption peak was observed at 3,313.09 $cm^{-1}$, corresponding to O–H stretching vibrations typically associated with phenolic and flavonoid compounds, which are key contributors to antioxidant activity [53,54]. Another significant peak appeared at 2,927.85 $cm^{-1}$, indicating aliphatic C–H stretching vibrations from long hydrocarbon chains, suggestive of organosulfur constituents such as allicin, diallyl disulfide (DADS), and diallyl trisulfide (DATS) [30,54]. Additionally, the peak at 1,042.56 $cm^{-1}$ can be attributed to C–O or C–S stretching vibrations, confirming the presence of ether or thiosulfonate groups, often linked to antimicrobial and anti-inflammatory activities [29,55]. The overall spectral pattern confirms the abundance of bioactive groups in SAG that are chemically compatible with vesicle-forming lipids. These findings provide a reference baseline for assessing molecular interactions following the encapsulation process.

The FTIR spectrum of the blank transfersome formulation (T-0) reflects the characteristic chemical architecture of its lipid and surfactant components, primarily soy phosphatidylcholine and sodium deoxycholate. As presented in **Figure 4** (black line) and detailed in **Table 2**, the peak at 3,305.96 $cm^{-1}$ corresponds to O–H stretching, which originates from the hydrophilic head groups of the phospholipids and surfactants [22,55]. The symmetric and asymmetric stretching vibrations of aliphatic C–H groups are evident at 2,853.85 and 2,923.73 $cm^{-1}$, representing the hydrocarbon chains within the lipid bilayer [56,57]. Ester functional groups related to the phospholipid backbone were observed at 1,062.53 and 1,226.56 $cm^{-1}$, while peaks at 851.45 and 521.99 $cm^{-1}$ are linked to aliphatic chain deformation and organosulfur-related fingerprint regions, respectively [54]. The absence of peaks specific to bioactive compounds from SAG indicates that this formulation comprises only the vesicle-forming matrix. This spectrum serves as a control reference to discern structural changes upon SAG incorporation.

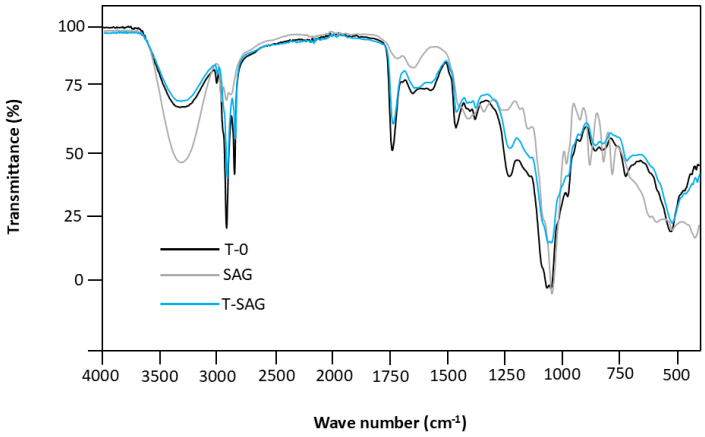


**Figure 4** FTIR spectra of T-0 (blank transfersome), SAG (crude single-aged garlic extract), and T-SAG (SAG-loaded transfersome) in the 4,000 - 500 $cm^{-1}$ range. Key SAG bands, including O–H (~3,400 $cm^{-1}$) and S=O/C–O (~1,030 - 1,100 $cm^{-1}$), are retained in T-SAG with minor shifts, supporting encapsulation. Altered band intensities suggest interactions between SAG and the vesicle matrix, while similar lipid-region features to T-0 indicate preserved vesicle integrity.

Following the incorporation of SAG extract into the transfersomal system, the T-SAG EA spectrum displayed distinct shifts in peak positions and intensities, evidencing molecular interactions between the extract's active constituents and the lipid bilayer. As shown in **Figure 4** (blue line) and **Table 2**, the O–H stretching peak shifted to 3,385.83 $cm^{-1}$, suggesting hydrogen bonding between SAG polyphenols and phospholipid polar heads [22]. The C–H stretching band shifted slightly to 2,932.75 $cm^{-1}$, indicating integration of SAG's aliphatic compounds into the lipid matrix [56]. Notably, the C–O/C–S band shifted from 1,042.56 $cm^{-1}$ (SAG) to 1,046.84 $cm^{-1}$ in T-SAG, signifying interaction between organosulfur compounds and the phospholipid structure [54]. Additional changes were observed in the ester linkage and aliphatic deformation regions, particularly at 1,227.97 and 974.10 $cm^{-1}$, confirming the successful embedding of SAG molecules within the bilayer. These spectral modifications indicate that the chemical structure of T-SAG remained intact while effectively encapsulating SAG's bioactive constituents, thereby supporting the stability and functionality of the delivery system.

**Table 2** FTIR peak comparison of transfersomes with and without SAG extract.

| Wavenumber ($cm^{-1}$) | SAG Functional Group | T-0 Functional Group | T-SAG Functional Group | Functional Group Assignment |
|---|---|---|---|---|
| 3,313.09 | –OH stretching | 3,305.96 | 3,385.83 | O–H stretching (phenol/alcohol) |
| 2,927.85 | C–H stretching | 2,923.73 | 2,932.75 | Aliphatic C–H stretching |
| 1,727.73 | – | 1,728.55 | – | C=O stretching (ester/lipid) |
| 1,042.56 | C–O/C–S stretching | 1,062.53 | 1,046.84 | C–O/C–S vibration (organosulfur/phospholipid) |
| 1,226.56 | – | 1,226.56 | 1,227.97 | C–O–C (ester linkage/phospholipid backbone) |
| 972.68 | – | 972.68 | 974.10 | C–H deformation (aliphatic chain stability) |
| 851.45 | – | 851.45 | 854.30 | C–H vibration (aliphatic region) |
| 521.99 | – | 521.99 | 520.57 | C–O/C–S (fingerprint region/organosulfur) |

Note: T-0 (blank transfersome); SAG (crude single-aged garlic extract); T-SAG (SAG-loaded transfersome).

**Encapsulation Efficiency (EE)**

EE is a key parameter that reflects the ability of a delivery system to entrap bioactive compounds and preserve their functionality throughout storage and application [57]. In this study, EE was determined based on the TPC, considering that phenolic compounds represent the major active constituents in SAG extract [58]. The use of TPC as a marker for EE is appropriate, as phenolics are primarily responsible for the antioxidant and pharmacological activity of SAG. Therefore, their encapsulation reflects the efficiency of the transfersome system in delivering the therapeutic potential of the extract. The EE of the T-SAG formulation was found to be 77.04 ± 6.62%, indicating that the majority of phenolic compounds were successfully entrapped within the vesicular structure. This value falls within the high efficiency range reported for transfersomal systems, typically ranging from 31% to 78% depending on the nature of the compound and preparation method [59]. While several comparative studies have reported EE values for synthetic compounds or pure drugs, such as N-acetylcysteine (59.78% – 65.58%) [60], the use of a crude extract in this study, which contains a diverse mixture of hydrophilic and lipophilic components, makes the result particularly notable [58]. This suggests that the formulation strategy effectively accommodated the complex nature of SAG extract. The relatively high EE observed can be attributed to the lipid composition and the presence of sodium deoxycholate as the edge activator. Surfactants with low hydrophilic-lipophilic balance (HLB) values, such as sodium deoxycholate, tend to enhance the encapsulation of lipophilic constituents [61]. However, the concentration of such edge activators must be carefully controlled, as excessive amounts (> 10%) can compromise membrane integrity and reduce entrapment efficiency [62]. Furthermore, higher surfactant concentrations (> 15%) may promote micelle formation, competing with vesicle assembly and reducing EE [16].

The loading capacity (LC) of the T-SAG formulation was 4.76%, indicating the proportion of phenolic content encapsulated per total mass of the formulation. This value is higher than those reported in some previous studies; for example, Luiz (2021) documented LC values of 1.25% - 1.29% for d-α-tocopheryl polyethylene glycol succinate (TPGS)-folate-modified transfersomes loaded with docetaxel [59]. TPGS is a commonly used surfactant for enhancing solubility and stability of poorly water-soluble drugs [59]. The higher LC in the T-SAG formulation may be due to the favorable interaction between SAG phenolics and the phospholipid bilayer, particularly the phosphatidylcholine matrix with suitable acyl chain characteristics [16]. Additionally, lipids with shorter acyl chains and lower transition temperatures (Tc) provide more fluid bilayers, enhancing entrapment and retention of hydrophobic compounds [61]. The combination of phosphatidylcholine, ethanol (as a membrane fluidizer), and sodium deoxycholate in the T-SAG formulation likely facilitated a stable and deformable bilayer structure that promoted high entrapment and loading efficiency. These results support the potential of T-SAG transfersomes as effective carriers for transdermal delivery of phenolic-rich herbal extracts, offering both high encapsulation and payload capacity for therapeutic applications.

**Total Phenol Content (TPC), Total Flavonoid Content (TFC), and antioxidant activity**

The T-SAG was developed to enhance the stability and bioavailability of phytochemicals found in aged garlic extract through transdermal delivery. This vesicular system comprises soy phosphatidylcholine as the primary structural lipid and sodium deoxycholate as an edge activator, enabling the formation of flexible, nanoscale lipid bilayers [1]. Ethanol functions as a membrane fluidizer, improving bilayer fluidity and compound entrapment, while phosphate-buffered saline (PBS) facilitates hydration and vesicle formation [38]. SAG itself is a rich source of bioactive compounds, particularly phenolic acids and flavonoids, which contribute to its known antioxidant potential [24]. The TPC of T-SAG was determined to be 62.19 ± 1.07 mg GAE/g (**Table 3**), confirming the effective incorporation of phenolic compounds into the transfersomal matrix [23]. Phenolic acids are major antioxidant constituents in garlic, capable of neutralizing reactive oxygen species (ROS) and preventing oxidative cellular damage [63]. Their successful encapsulation is supported by the high EE of

77.04 ± 6.62%, which reflects the capacity of the vesicular system to protect these molecules during formulation. This is further reinforced by the favorable particle characteristics of T-SAG, which include a nanometric size of 81.03 ± 0.47 nm and a narrow PDI of 0.140 ± 0.008 at initial storage, parameters essential for colloidal stability and transdermal penetration.

**Table 3** Total flavonoid content, total phenolic content, and antioxidant activity of T-SAG.

| Parameter | Value |
|---|---|
| Total Phenol Content (mg GAE/g) | 62.19 ± 1.07 |
| Total Flavonoid Content (mg QE/g) | 63.15 ± 0.38 |
| Antioxidant activity (%) | 77.74 ± 2.88 |

Note: T-SAG (Transfersomes Single-Aged Garlic)

In addition, the TFC was measured at 63.15 ± 0.38 mg QE/g (**Table 3**), highlighting the presence of another important class of phytochemicals in SAG. Flavonoids such as quercetin, kaempferol, and their derivatives have well-documented roles as antioxidants, with the ability to donate electrons and chelate metal ions [23]. The structural composition of T-SAG, including the amphiphilic nature of phospholipids and the presence of sodium deoxycholate, supports efficient loading of both hydrophilic and lipophilic flavonoids [23]. These findings suggest that the formulation system maintains the integrity of flavonoid compounds and enhances their delivery efficiency. The antioxidant activity of T-SAG was evaluated using the DPPH free radical scavenging method and exhibited a strong inhibition value of 77.74 ± 2.88% (**Table 3**), indicating preserved antioxidant functionality of the encapsulated compounds. The high level of antioxidant activity is directly associated with the phenolic and flavonoid content, confirming that the transfersome system successfully retains the redox-active properties of SAG phytoconstituents. Moreover, the measured LC of 4.76% reflects the capability of the formulation to incorporate a meaningful amount of bioactive extract relative to its total mass, which is essential for achieving therapeutic concentrations upon administration.

The antioxidant mechanism of T-SAG is primarily attributed to the presence of phenolic and flavonoid compounds, which act through hydrogen atom donation, electron transfer, and metal ion chelation. Phenolic acids such as gallic acid and caffeic acid neutralize free radicals by donating hydrogen atoms from their hydroxyl groups, thereby terminating radical chain reactions [23]. Flavonoids like quercetin and kaempferol contribute to redox homeostasis by ROS through conjugated double bonds and hydroxyl substitutions on their aromatic rings [64,65]. These interactions not only inhibit oxidative damage to cellular lipids, proteins, and DNA but also regenerate endogenous antioxidants such as glutathione [66]. Encapsulation in transfersomes enhances the solubility and cellular uptake of these bioactive compounds, enabling them to exert their protective effects more efficiently at the target site.

**Antibacterial activity assay**

The antibacterial activity of the T-SAG formulation was evaluated to examine its inhibitory potential against representative Gram-negative and Gram-positive bacteria, namely *P. aeruginosa*, *E. coli*, and *S. aureus*. The assessment was performed using the agar diffusion method on Mueller-Hinton Agar (MHA), which provides a preliminary indication of antibacterial activity based on inhibition zone formation but does not directly quantify bactericidal or bacteriostatic potency. T-SAG was applied at concentrations of 7.5, 10, and 12.5 mg/mL, while chloramphenicol served as a positive control (**Table 4**). As summarized in **Table 4**, T-SAG exhibited concentration-dependent inhibitory effects against all tested strains, as reflected by measurable inhibition zones. The largest inhibition zone was observed against *E. coli* (8.19 ± 1.34 mm), followed by *S. aureus* (7.25 ± 0.20 mm), whereas *P. aeruginosa* demonstrated the lowest susceptibility (6.59 ± 0.25 mm). Although these inhibition zones were significantly smaller than those produced by chloramphenicol (**p** <

0.05), the consistent increase in inhibition zone diameter with increasing T-SAG concentration indicates a measurable antibacterial response. However, this activity should be interpreted as moderate and preliminary rather than equivalent to that of conventional antibiotics.

**Table 4** Antibacterial activity of T-SAG against selected bacterial strains.

| Treatment | Inhibition Zone Diameter (mm) | | |
|---|---|---|---|
| | ***P. aeruginosa*** | ***E. coli*** | ***S. aureus*** |
| T-SAG 7.5 mg/mL | 6.44 ± 0.37[a] | 6.73 ± 0.68[a] | 6.67 ± 0,54[a] |
| T-SAG 10 mg/mL | 6.55 ± 0.37[a] | 7.44 ± 1.15[a] | 6.68 ± 0.22[a] |
| T-SAG 12.5 mg/mL | 6.59 ± 0.25[a] | 8.19 ± 1.34[a] | 7.25 ± 0.2[a] |
| Chloramphenicol | 9.58 ± 1.03[b] | 31.13 ± 0.61[b] | 29.63 ± 1.12[b] |

Note: T-SAG (Transfersomes Single-Aged Garlic)

As summarized in **Table 4**, T-SAG exhibited concentration-dependent inhibitory effects against all tested strains, as reflected by measurable inhibition zones. The largest inhibition zone was observed against *E. coli* (8.19 ± 1.34 mm), followed by *S. aureus* (7.25 ± 0.20 mm), whereas *P. aeruginosa* demonstrated the lowest susceptibility (6.59 ± 0.25 mm). Although these inhibition zones were significantly smaller than those produced by chloramphenicol ($p < 0.05$), the consistent increase in inhibition zone diameter with increasing T-SAG concentration indicates a measurable antibacterial response. However, this activity should be interpreted as moderate and preliminary rather than equivalent to that of conventional antibiotics [23,67]. In addition, organosulfur compounds such as allicin, diallyl disulfide (DADS), and diallyl trisulfide (DATS) are known to interact with thiol-containing enzymes, thereby disrupting key bacterial metabolic pathways [68,69]. The combined presence of these compounds likely contributes synergistically to the observed antibacterial activity of T-SAG.

Differences in bacterial susceptibility among the tested strains can be explained by variations in cell wall and membrane architecture. P. aeruginosa exhibited the lowest sensitivity, which is consistent with its intrinsically resistant outer membrane rich in lipopolysaccharides (LPS) and its low membrane permeability, limiting the diffusion of antibacterial agents [70,71]. In contrast, *E. coli*, although also Gram-negative, showed higher susceptibility, potentially due to differences in outer membrane composition and relatively greater membrane fluidity [72]. *S. aureus, a Gram-positive bacterium lacking an LPS barrier, allows relatively easier access of lipophilic compounds through its thick peptidoglycan layer* [73]. The transfersomal carrier system may further influence antibacterial performance by facilitating closer interaction between encapsulated bioactives and bacterial cell membranes. The nanoscale particle size, relatively narrow PDI, and high encapsulation efficiency of T-SAG support improved dispersion and surface contact with bacterial cells, potentially enhancing local bioactive availability. The amphiphilic nature of phosphatidylcholine and sodium deoxycholate enables the vesicles to accommodate both hydrophilic and lipophilic compounds [74]. Nevertheless, it should be emphasized that inhibition zone size in agar diffusion assays is influenced by diffusion behavior and does not fully reflect antibacterial efficacy under physiological or clinical conditions.

The antibacterial activity observed in this study should be regarded as indicative of the supportive role of the transfersomal system in preserving and delivering SAG bioactives, rather than as evidence of strong or clinically comparable antibacterial potency. Further investigations using quantitative assays such as minimum inhibitory concentration (MIC), time-kill kinetics, and *in vivo* infection models are required to more accurately determine the antibacterial effectiveness and therapeutic relevance of the T-SAG formulation.

## Conclusions

The transfersome-based formulation of single-aged garlic extract (T-SAG) was successfully developed and characterized, demonstrating suitable physicochemical properties, preserved bioactive compounds, and measurable antioxidant and antibacterial activities. Morphological and spectroscopic analyses confirmed vesicle formation and compatibility between the extract and formulation components, while encapsulation efficiency supported the effective entrapment of phenolic- and flavonoid-rich constituents. Although the formulation exhibited promising *in vitro* bioactivity, the findings are limited by storage stability issues and the use of *in vitro* antioxidant and antibacterial assays, which do not fully represent *in vivo* performance. Overall, this study provides preliminary evidence that transfersome encapsulation enhances the functional stability and bioactivity of single-aged garlic extract, supporting its potential development as a natural topical antimicrobial system, pending further optimization and biological validation.

## Acknowledgements

We would like to express our deepest gratitude for the generous funding support provided by the Universitas Negeri Malang PNBP, Indonesia grant under the Matching Fund Scheme, contract number: 4.4.655/UN32.14.1/LT/2024. This support has been instrumental in enabling our research and furthering our commitment to academic excellence.

## Declaration of generative AI in scientific writing

The authors acknowledge the use of generative AI tools (e.g., QuillBot and Grammarly) in the preparation of this manuscript, limited to language refinement and grammatical correction. No AI-assisted content generation, data analysis, or interpretation was undertaken. The authors assume full responsibility for the accuracy, integrity, and conclusions presented herein.

## Credit author statement

**Sri Rahayu Lestari**: Conceptualization, Methodology, Supervision, Writing - Review & Editing. **Dewi Sekar Miasih**: Investigation, Data Curation, Writing - Original Draft, Visualization. **Alif Rosyidah El Baroroh**: Investigation, Data Curation, Formal Analysis, Visualization. **Yuslinda Annisa**: Investigation, Data Curation, and Formal Analysis. **Muhammad Mauludi Zulkifli**: Investigation, Data Curation, and Formal Analysis. **Abdul Gofur**: Conceptualization, Methodology, Supervision, Formal Analysis. **Yunita Rakhmawati**: Methodology, Formal Analysis, Investigation, Writing - Original Draft. **Suharti**: Investigation, and Data Curation. **Nik Ahmad Nizam Nik Malek**: Resources, Funding Acquisition, Writing - Review & Editing.

## References

[1] V Singh, S Dharashivkar, M Gaikwad and S Shaikh. Development and evaluation of transferosomal gel using cephalexin. *Research Square* 2021. https://doi.org/10.21203/rs.3.rs-940323/v1

[2] J Zakhour, SL Sharara, JR Hindy, SF Haddad and SS Kanj. Antimicrobial treatment of *Pseudomonas aeruginosa* severe sepsis. *Antibiotics* 2022; **11(10)**, 1-19.

[3] CJL Murray, KS Ikuta, F Sharara, L Swetschinski, G Robles Aguilar, A Gray, C Han, C Bisignano, P Rao, E Wool, SC Johnson, AJ Browne, MG Chipeta, F Fell, S Hackett, G Haines-Woodhouse, BH Kashef Hamadani, EAP Kumaran, B McManigal, …, M Naghavi. Global burden of bacterial antimicrobial resistance in 2019: A systematic analysis. *The Lancet* 2022; **399(10325)**, 629-655.

[4] T Astuti, PR Novitasari, R Tjandrawinata, AE Nugroho and S Pramono. Anti-diabetic effect of andrographolide from sambiloto herbs (*Andrographis paniculata* (Burm.f.) Nees) through the expression of PPARγ and GLUT-4 in adipocytes. *Indonesian Journal of Biotechnology* 2022; **27(4)**, 203-211.

[5] GMC De Macedo, S Nunes and T Barreto. Skin disorders in diabetes mellitus: An epidemiology and physiopathology review. *Diabetology & Metabolic Syndrome* 2016; **8(1)**, 1-8.

[6] VM Musyoki, W Mutai, N Ngugi, F Otieno and MM Masika. Speciation and antifungal susceptibility of Candida isolates from diabetic foot ulcer patients in a tertiary hospital in Kenya. *Pan African Medical Journal* 2022; **41(1)**, 34.

[7] S Rasoulpoor, S Shohaimi, N Salari, A Vaisi-Raygani, S Rasoulpoor, S Shabani, R Jalali and M Mohammadi. Candida albicans skin infection in patients with type 2 diabetes: A systematic review and meta-analysis. *Journal of Diabetes & Metabolic Disorder*s 2021; **20(1)**, 665-672.

[8] M Falcone, JJ Meier, MG Marini, R Caccialanza, JM Aguado, S Del Prato and F Menichetti. Diabetes and acute bacterial skin and skin structure infections. *Diabetes Research and Clinical Practice* 2021; **174**, 108732.

[9] WT Chang, JL Lim and CL Hsu. Inhibitory effect of methanolic extract of black garlic on adipogenesis in 3T3-L1 adipocytes. *Chung Shan Medical Journal* 2018; **29(2)**, 113-121.

[10] RCMR Nassur, EVB Vilas Boas and FV Resende. Black garlic: Transformation effects, characterization and consumer purchase intention. *Comunicata Scientiae* 2017; **8(3)**, 444-451.

[11] P Sunanta, V Kontogiorgos, T Pankasemsuk, K Jantanasakulwong, P Rachtanapun, P Seesuriyachan and SR Sommano. The nutritional value, bioactive availability and functional properties of garlic and its related products during processing. *Frontiers in Nutrition* 2023; **10**, 1142784.

[12] SN Handayani, LC Bawono, DP Ayu and HN Pratiwi. Isolasi senyawa polifenol black garlic dan uji toksisitasnya terhadap larva udang (*Artemia salina* Leach). *Jurnal Ilmu Kefarmasian Indonesia* 2018; **16(2)**, 145-149.

[13] S Roy, F Hussain and N Mazumder. Understanding the potential of black garlic as an antibacterial agent by quantifying volume scattering function. *Discover Applied Sciences* 2025; **7(4)**, 235.

[14] LH Muharram, FN Syaputri, W Pertiwi and RF Saputri. Antibacterial activity of black garlic extract variations in aging time on prevention of skin dysbiosis causes acne. *Jurnal Sains dan Kesehatan* 2022; **4(2)**, 181-188.

[15] NZ Darajat, A Chaerunisaa and M Abdassah. Transfersome as topical drug delivery: formulation and characterization. *Jurnal Farmasi Galenika* 2023; **9(1)**, 41-54.

[16] AA Miatmoko, NA Marufah, Q Nada, N Rosita, T Erawati, J Susanto, KE Purwantari, A Nurkanto, Purwati and W Soeratri. The effect of surfactant type on characteristics, skin penetration and anti-aging effectiveness of transfersomes containing amniotic mesenchymal stem cells metabolite products in UV-aging induced mice. *Drug Delivery* 2022; **29(1)**, 3443-3453.

[17] A Leonyza and S Surini. Optimization of sodium deoxycholate-based transfersomes for percutaneous delivery of peptides and proteins. *International Journal of Applied Pharmaceutics* 2019; **11(5)**, 329-332.

[18] MI Khan, S Yaqoob, A Madni, MF Akhtar, MF Sohail, A Saleem, N Tahir, K Khan and OS Qureshi. Development and in *vitro*/*ex vivo* evaluation of lecithin-based deformable transfersomes and transfersome-based gels for combined dermal delivery of meloxicam and dexamethasone. *BioMed Research International* 2022; **2022(1)**, 8170318.

[19] AC Khayrani, M Fahmi, RW Nurhayati, NHA Manas and M Suhaeri. Effect of freeze-thaw cycles method to transfersome characteristics for growth protein encapsulation. *International Journal of Technology* 2024; **15**, 267-278.

[20] A Wongrakpanich, J Leanpolchareanchai, B Morakul, W Parichatikanond and V Teeranachaideekul. Phyllanthus emblica extract-loaded transfersomes for hair follicle targeting: Phytoconstituents, characterization, and hair growth promotion. *Journal of Oleo Science* 2022; **71(7)**, 1085-1096.

[21] W Wang, KJ Lu, CH Yu, QL Huang and YZ Du. Nano-drug delivery systems in wound treatment and skin regeneration. *Journal of Nanobiotechnology* 2019; 1**7(1)**, 82.

[22] KS Avadhani, J Manikkath, M Tiwari, M Chandrasekhar, A Godavarthi, SM Vidya, RC Hariharapura, G Kalthur, N Udupa and S Mutalik. Skin delivery of epigallocatechin-3-gallate (EGCG) and hyaluronic acid loaded nano-transfersomes for antioxidant and anti-aging effects in UV radiation induced skin damage. *Drug Delivery* 2017; **24(1)**, 61-74.

[23] HB Hmad, N Sellami, HB Jemaa and MM Lasram. Therapeutic and biological properties of white garlic and black garlic extracts (*Allium sativum* L.): A comparative analysis. *Journal of Medicinal Food* 2025; **28(8)**, 768-775.

[24] MA Harun, S Buraena, EA Wello, HH Idrus and

ASF Arsal. Antibacterial potency of black garlic extract from *Allium sativum* on *Escherichia coli*. *Green Medical Journal* 2021; **3(3)**, 124-131.

[25] T Jiang, T Wang, T Li, Y Ma, S Shen, B He and R Mo. Enhanced transdermal drug delivery by transfersome-embedded oligopeptide hydrogel for topical chemotherapy of melanoma. *ACS Nano* 2018; **12(10)**, 9693-9701.

[26] M Danaei, M Dehghankhold, S Ataei, FH Davarani, R Javanmard, A Dokhani, S Khorasani and MR Mozafari. Impact of particle size and polydispersity index on the clinical applications of lipidic nanocarrier systems. *Pharmaceutics* 2018; **10(2)**, 57.

[27] I Iskandarsyah, AD Rahmi and DM Pangesti. Comparison of the characteristics of transfersomes and protransfersomes containing azelaic acid. *Journal of Young Pharmacists* 2018; **10(2)**, s11-s15.

[28] U Varia, D Joshi, M Jadeja, H Katariya, K Detholia and V Soni. Development and evaluation of ultradeformable vesicles loaded transdermal film of boswellic acid. *Future Journal of Pharmaceutical Sciences* 2022; **8(1)**, 39.

[29] SR Lestari, A Ghofur, SI Maslikah, Sunaryono, AN Rahma, DN Aisyah, IN Mufidah, ND Rifqi, N Prastita, DS Miasih and AR El Baroroh. Profiling of single garlic extract microencapsulation: Characterization, antioxidant activity, and release kinetic. *Journal of Tropical Biodiversity and Biotechnology* 2023; **8(3)**, jtbb79072.

[30] SR Lestari, A Gofur, Hartatiek, Y Annisa, DN Ramadhani, AN Rahma, DN Aisyah, IN Mufidah and ND Rifqi. Characterization and *in-vitro* study of micro-encapsulation chitosan alginate of single-bulb garlic extract. *Pharmaceutical Nanotechnology* 2024; **12(2)**, 155-164.

[31] D Praseptiangga, HL Zahara, PI Widjanarko, IM Joni and C Panatarani. Preparation and FTIR spectroscopic studies of SiO2-ZnO nanoparticles suspension for the development of carrageenan-based bio-nanocomposite film. *AIP Conference Proceedings* 2020; **2219(1)**, 100005.

[32] M Tagrida, T Prodpran, B Zhang, RE Aluko and S Benjakul. Liposomes loaded with betel leaf (*Piper betle* L.) ethanolic extract prepared by thin film hydration and ethanol injection methods: characteristics and antioxidant activities. *Journal of Food Biochemistry* 2021; **45(12)**, e14012.

[33] N Hadidi, M Saffari and M Faizi. Optimized transferosomal bovine lactoferrin (BLF) as a promising novel non-invasive topical treatment for genital warts caused by human papiluma virus (HPV). I*ranian Journal of Pharmaceutical Research* 2018; **17(SI 2)**, 12-23.

[34] NNA Dewi and IW Mustika. Nutrition content and antioxidant activity of black garlic. *International Journal of Health Sciences* 2018; **2(1)**, 11-20.

[35] Y Wasihun, HA Habteweld and KD Ayenew. Antibacterial activity and phytochemical components of leaf extract of *Calpurnia aurea*. *Scientific Reports* 2023; **13(1)**, 9767.

[36] A Nasr, A Gardouh and M Ghorab. Novel solid self-nanoemulsifying drug delivery system (S-SNEDDS) for oral delivery of olmesartan medoxomil: Design, formulation, pharmacokinetic and bioavailability evaluation. *Pharmaceutics* 2016; **8(3)**, 20.

[37] M Ghazwani, MH Alqarni, U Hani and A Alam. QbD-optimized, phospholipid-based elastic nanovesicles for the effective delivery of 6-gingerol: A promising topical option for pain-related disorders. *International Journal of Molecular Sciences* 2023; **24(12)**, 9983.

[38] H Natsheh and E Touitou. Phospholipid vesicles for dermal/transdermal and nasal administration of active molecules: The effect of surfactants and alcohols on the fluidity of their lipid bilayers and penetration enhancement properties. *Molecules* 2020; **25(13)**, 2959.

[39] BR Shah, C Zhang, Y Li and B Li. Bioaccessibility and antioxidant activity of curcumin after encapsulated by nano and Pickering emulsion based on chitosan-tripolyphosphate nanoparticles. *Food Research International* 2016; **89**, 399-407.

[40] A Altan, HB Yuce, Ő Karataş, MM Taşkan, F Gevrek, S Çolak and N Akbulut. Free and liposome form of gallic acid improves calvarial bone wound healing in Wistar rats. *Asian Pacific Journal of Tropical Biomedicine* 2020; **10(4)**, 156-163.

[41] I Khan, R Needham, S Yousaf, C Houacine, Y Islam, R Bnyan, SK Sadozai, MA Elrayess and A Elhissi. Impact of phospholipids, surfactants and cholesterol selection on the performance of transfersomes vesicles using medical nebulizers

for pulmonary drug delivery. *Journal of Drug Delivery Science and Technology* 2021; **66**, 102822.

[42] AN Rahma, DN Aisyah, Y Annisa, A Gofur, SI Maslikah and SR Lestari. Characterization and hemocompatibility assay of microencapsulation chitosan-alginate single garlic extract-loaded (MCA-SGE). *BIO Web of Conferences* 2024; **117**, 01011.

[43] DS Miasih, Y Annisa, SR Lestari, H Susanto and S Sunaryono. Novel self-nanoemulsifying drug delivery system of single bulb garlic: stability, toxicity, and antiinflammation in 3T3-L1 cells. *Science and Technology Indonesia* 2022; **7(4)**, 417-426.

[44] U Sundralingam, S Muniyandy, AK Radhakrishnan and UD Palanisamy. Ratite oils for local transdermal therapy of 4-OH tamoxifen: Development, characterization, and ex vivo evaluation. *Journal of Liposome Research* 2021; **31(3)**, 217-229.

[45] MK Amin and JS Boateng. Enhancing stability and mucoadhesive properties of chitosan nanoparticles by surface modification with sodium alginate and polyethylene glycol for potential oral mucosa vaccine delivery. *Marine Drugs* 2022; **20(3)**, 156.

[46] V Popovici, L Bucur, CE Gîrd, D Rambu, SI Calcan, EI Cucolea, T Costache, M Ungureanu-Iuga, M Oroian, S Mironeasa, V Schröder, EA Ozon, D Lupuliasa, A Caraiane and V Badea. Antioxidant, cytotoxic, and rheological properties of canola oil extract of *Usnea barbata* (L.) Weber ex F.H. Wigg from Călimani Mountains, Romania. *Plants* 2022; **11(7)**, 854.

[47] D Lombardo and MA Kiselev. Methods of liposomes preparation: Formation and control factors of versatile nanocarriers for biomedical and nanomedicine application. *Pharmaceutics* 2022; **14(3)**, 543.

[48] MC Tanzi, S Farè and G Candiani. *Techniques of analysis*. *In*: MC Tanzi, S Farè and G Candiani (Eds.). Foundations of biomaterials engineering. Academic Press, New York, 2019, p. 393-469.

[49] A Wongrakpanich, J Leanpolchareanchai, B Morakul, W Parichatikanond and V Teeranachaideekul. Phyllanthus emblica extract-loaded transfersomes for hair follicle targeting: Phytoconstituents, characterization, and hair growth promotion. *Journal of Oleo Scienc*e 2022; **71(7)**, 1085-1096.

[50] MJ Masarudin, SM Cutts, BJ Evison, DR Phillips and PJ Pigram. Factors determining the stability, size distribution, and cellular accumulation of small, monodisperse chitosan nanoparticles as candidate vectors for anticancer drug delivery: Application to the passive encapsulation of [14C]-doxorubicin. *Nanotechnology, Science and Applications* 2015; **8**, 67-80.

[51] R Squittieri, L Baldino and E Reverchon. Production of antioxidant transfersomes by a supercritical CO2 assisted process for transdermal delivery applications. *Nanomaterials* 2023; **13(12)**, 1812.

[52] V Singh, S Dharashivkar, M Gaikwad and S Shaikh. Development and evaluation of transferosomal gel using cephalexin. *Research Square* 2021. https://doi.org/10.21203/rs.3.rs-940323/v1

[53] MA Siregar, JA Santri, D Aksani, A Maas and M Nurudin. Analysis of FTIR spectroscopic data to observe hydrophilic and hydrophobic levels of peat in hemic and sapric maturity. I*OP Conference Series: Earth and Environmental Science* 2022; **1025(1)**, 012026.

[54] BJ Divya, B Suman, M Venkataswamy and K Thyagaraju. A study on phytochemicals, functional groups and mineral composition of *Allium sativum* (garlic) cloves. *International Journal of Current Pharmaceutical Research* 2017; **9(3)**, 42-45.

[55] NA Ramli, N Ali, S Hamzah and NI Yatim. Physicochemical characteristics of liposome encapsulation of stingless bees' propolis. *Heliyon* 2021; **7(4)**, e06649.

[56] M Mecozzi and E Sturchio. Computer assisted examination of infrared and near infrared spectra to assess structural and molecular changes in biological samples exposed to pollutants: A case of study. *Journal of Imaging* 2022; **3(1)**, 11.

[57] A Motawea, SN Maria, DN Maria, MM Jablonski and MM Ibrahim. Genistein transfersome-embedded topical delivery system for skin melanoma treatment: *In vitro* and *ex vivo* evaluations. *Drug Delivery* 2024; **31(1)**, 2372277.

[58] MA Hashim, X Huang, LA Nadtochii, DA

Baranenko, MS Boulkrane and TM El-Messery. Encapsulation of bioactive compounds extracted from date palm seeds (*Phoenix dactylifera* L.) and their use in functional food. *Frontiers in Nutrition* 2022; **9**, 1051050.

[59] MT Luiz, L Abriata, JCR de Castro, JR Rocha, C de Tognon, JM Marchetti, G de Oliveira, CP de Sousa and CLM de Castro. Docetaxel-loaded folate-modified TPGS-transfersomes for glioblastoma multiforme treatment. *Materials Science and Engineering: C* 2021; **124**, 112033.

[60] HH Harmita, I Iskandarsyah and SF Afifah. Effect of transfersome formulation on the stability and antioxidant activity of N-acetylcysteine in anti-aging cream. *International Journal of Applied Pharmaceutics* 2020; **12(1)**, 156-162.

[61] S Potisuwan, N Apichatwatana and S Rujivipat. Improved skin permeation of transferosomes containing Eulophia macrobulbon extract. *Colloids and Surfaces B: Biointerfaces* 2023; **229**, 113474.

[62] PS Wu, YS Li, YC Kuo, SJJ Tsai and CC Lin. Preparation and evaluation of novel transfersomes combined with the natural antioxidant resveratrol. *Molecules* 2019; **24(3)**, 600.

[63] T Ahmed and CK Wang. Black garlic and its bioactive compounds on human health diseases: A review. *Molecules* 2021; **26(16)**, 5028.

[64] J Rohmah. Antioxidant activities using DPPH, FIC, FRAP, and ABTS methods from ethanolic extract of lempuyang gajah rhizome (*Zingiber zerumbet* (L.) Roscoe ex Sm.). *Jurnal Kimia Riset* 2022; **7(2)**, 152-166.

[65] GS Prihanti, F Isnaini, R Yudistia, A Faradilla and M Rahman. Effect of black garlic extract on blood glucose, lipid profile, and SGPT-SGOT of wistar rats diabetes mellitus model. *Majalah Kedokteran Bandun*g 2019; **51(2)**, 82-87.

[66] EOJ La, KR Pandi and NK Esati. Aktivitas antibakteri fraksi ekstrak black garlic terhadap bakteri Propionibacterium acnes dengan metode difusi cakram. *Health Science and Pharmaceutical Journal* 2022; **6(3)**, 87-96.

[67] E Lemma, Z Yusuf, M Desta, S Seyida, M Idris, S Mengistu and J Teneshu. Physicochemical properties and biological activities of Garlic (*Allium sativum* L.) bulb and leek (*Allium ampeloprasum* L. var. Porrum) leaf oil extracts. *The Scientific World Journal* 2022; **2022**, 6573754.

[68] J Borlinghaus, F Albrecht, MCH Gruhlke, ID Nwachukwu and AJ Slusarenko. Allicin: Chemistry and biological properties. *Molecules* 2014; **19(8)**, 12591-12618.

[69] WA Cahayani, C Tanuwijaya, LX Chi and Y Mulyastuti. Antibacterial activity of garlic (*Allium sativum*) extract and molecular docking studies of allicin. *AIP Conference Proceedings* 2019; **2108(1)**, 020045.

[70] N Fitriana, AA Ainayya, FA Pamasyah, MA Anam and SR Lestari. The effectiveness comparison of single bulb garlic extract for antibacterial agent P. aeruginosa. *IOP Conference Series: Earth and Environmental Science* 2019; **276(1)**, 012028.

[71] B Coşkun, M Ayhan, S Ulusoy and R Guner. Bacterial profile and antimicrobial resistance patterns of diabetic foot infections in a major research hospital of Turkey. *Antibiotics* 2024; **13(7)**, 599.

[72] M Khalid, M Amayreh, S Sanduka, Z Salah, F Al-Rimawi, GM Al-Mazaideh, AA Alanezi, F Wedian, F Alasmari and MH Faris Shalayel. Assessment of antioxidant, antimicrobial, and anticancer activities of *Sisymbrium officinale* plant extract. *Heliyon* 2022; **8(9)**, e10477.

[73] A Gofur, I Wulandari, MF Athoillah, A Witjoro and SR Lestari. Single clove garlic (*Allium sativum*) essential oil as an inhibitor of Staphylococcus aureus bacteria. *Biosaintifika: Journal of Biology & Biology Education* 2019; **11(1)**, 77-83.

[74] OO Olatunde, S Benjakul, K Vongkamjan and T Amnuaikit. Influence of stabilising agents on the properties of liposomal encapsulated ethanolic coconut husk extract. *International Journal of Food Science & Technology* 2020; **55(2)**, 702-711.